PAPER

A dragline-forming mobile robot inspired by spiders

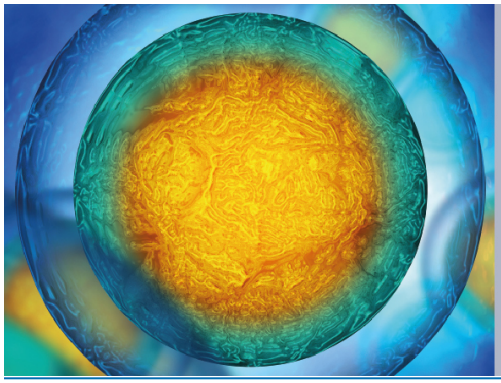

IOP Publishing Bioinspiration & Biomimetics
Bioinspir. Biomim. 9 (2014) 016006 (10pp) doi:10.1088/1748-3182/9/1/016006

A dragline-forming mobile robot inspired by spiders

Liyu Wang, Utku Culha and Fumiya Iida

Bio-Inspired Robotics Lab, ETH Zurich, Leonhardstrasse 27, 8092 Zurich, Switzerland

E-mail: liyu.wang@mavt.ethz.ch

Received 4 October 2013, revised 5 November 2013
Accepted for publication 13 November 2013
Published 16 January 2014

Abstract

Mobility of wheeled or legged machines can be significantly increased if they are able to move from a solid surface into a three-dimensional space. Although that may be achieved by addition of flying mechanisms, the payload fraction will be the limiting factor in such hybrid mobile machines for many applications. Inspired by spiders producing draglines to assist locomotion, the paper proposes an alternative mobile technology where a robot achieves locomotion from a solid surface into a free space. The technology resembles the dragline production pathway in spiders to a technically feasible degree and enables robots to move with thermoplastic spinning of draglines. As an implementation, a mobile robot has been prototyped with thermoplastic adhesives as source material of the draglines. Experimental results show that a dragline diameter range of 1.17–5.27 mm was achievable by the 185 g mobile robot in descending locomotion from the solid surface of a hanging structure with a power consumption of 4.8 W and an average speed of 5.13 cm min^{-1}. With an open-loop controller consisting of sequences of discrete events, the robot has demonstrated repeatable dragline formation with a relative deviation within −4% and a length close to the metre scale.

S Online supplementary data available from stacks.iop.org/BB/9/016006/mmedia

(Some figures may appear in colour only in the online journal)

1. Introduction

Mobile robots are useful machines for transportation, inspection, surveillance, hazard removal, environmental monitoring, extraterrestrial exploration, among other uses. Mobile robots should be able to move in the environment where the tasks are carried out, or even in unanticipated environments. Wheel-based and leg-based technologies have enabled robots to move on ground surfaces or terrains and to climb on stairs [1], poles [2], slopes, ceilings or vertical surfaces [3, 4]. However, it has not been possible for wheeled or legged robots to move away from solid surfaces into a three-dimensional space in a controlled way, without the assistance of an existing cable [5–8] or the capability of flying [9]. An existing cable requires the robot to carry a winch, and the total length of the cable is determined by its thickness and the size of the winch. In the case of flying, the payload fraction is an important issue but flying robots currently do not perform very satisfactorily.

In nature, certain terrestrial animals have the ability to move in a free-space in a controlled manner without flying. One of the representatives is spider, such as *Araneus* and *Nephila*. A spider moves away from a surface in the environment, such as a wall or a branch of a tree, into the free-space by producing draglines (see figure 1(*a*)). With this ability, the spider is able to reach another surface, capture a prey, or make a web and position itself on the surfaces of the web. Such behaviour may inspire design of wheeled or legged robots to extend their mobility into a free-space. Furthermore, studies have found that spiders with a larger body mass produce thicker draglines [10], and the thickness of draglines from a single spinneret can be varied by the spider [12]. The principle implies that, when implemented in a mobile robot with the dragline-forming capability, the robot may also control the thickness of draglines according to payload requirement. This will make the mobile robot capable of covering a large range of payloads. It will also make the robot advantageous over those using an existing cable with a winch in at least two ways. Firstly, given the same volume of dragline material as the cable in a winched robot, adjustable thickness means the robot may maximize the length of the dragline while not sacrificing the payload need; and secondly, the robot has higher chance

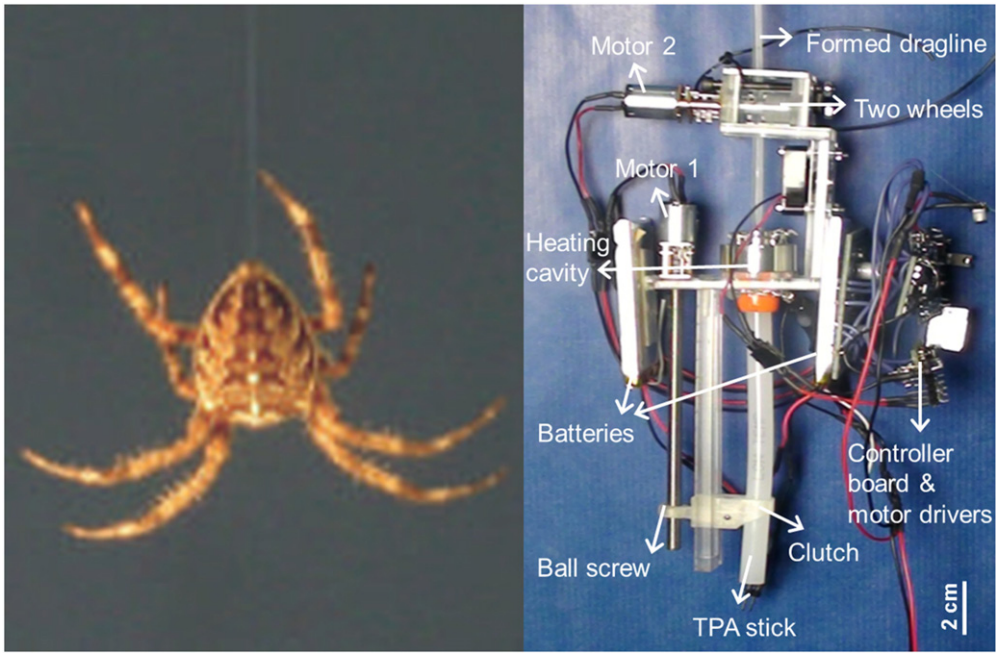

(*a*) (*b*)

Figure 1. (*a*) A falling spider (*Araneus*), reprinted by permission from Macmillan Publishers Ltd: [17], copyright 2006. (*b*) Front view of a mobile robot with draglines made of source material thermoplastic adhesives (TPAs). The extrusion mechanism (lower half of the robot) resembles the secretion in the major ampullate gland of spiders, and it is labelled in detail.

to adapt to a very large but unanticipated payload that may exceed the breaking tension of a given cable.

To enable a robot to move from a solid surface into the free space with dragline formation, technical challenges must be tackled since the robot must form a thread while moving without any other physical support than the thread itself. Spiders do so with the fourth pair of legs and the dragline spinneret, which includes the major ampullate gland and a related spinning duct. The dragline production pathway in the spinneret has been considerably studied [11, 12]. The major ampullate gland secretes the spinning protein dope and constitutes the main storage repository that leads to the duct. The duct is then responsible for fibre formation and terminates with a valve. After the valve, further processing proceeds in a narrow tubular region and the dragline thread then exits at the spigot. The pathway is mechanically similar to an industrial pultrusion system subject to an initial shear stress. The pulling force comes from the fourth pair of the legs of the spider and/or the gravitational force of the body mass. With such a process, spiders weighing a few hundred milligrams are able to produce draglines that are a few micrometres thick [10].

From the perspective of robotics, the demand for a combination of dragline formation and locomotion requires a robotic system to include source material that makes draglines. Furthermore, the source material must be able to change its strength so that it can be easily deformed into a dragline on the one hand and it gives strong physical support for locomotion on the other. In other words, phase transition of the source material is necessary. Spiders do so by liquid crystal spinning of draglines [13]. However, liquid crystal spinning requires sophisticated chemical techniques which could be implemented in biomaterial engineering [13, 14] but is beyond the feasibility as an onboard technique within a mobile robot.

The paper presents a dragline-forming mobile technology inspired by spiders. The technology is based on thermoplastic spinning with an extrusion process that resembles the secretion in the major ampullate gland and an open-air deformation process that resembles the pultrusion in the duct of the spiders. With thermoplastic spinning, phase transition can be easily modelled and controlled since strength dependence on temperature is universal for material. The technology is realized in a self-contained mobile robot with onboard batteries and source material of thermoplastic adhesives (TPAs). With a case study of vertical descending from the surface of a hanging structure into a free space, the robot demonstrates locomotion assisted by dragline formation with variable diameters.

TPAs are thermoplastics that have adhesion strength as high as several megapascal at room temperature. They have versatile applications and can be used to bond various adherends, from metals, plastics, glass, ceramics, rubbers, stone, to wood [15]. They are easily accessible and economical as proven in industries such as packaging, furniture, book binding, aerospace, etc. They have also been used in robotics as a general mechanism for automatic mechanical connection and disconnection between macroscopic parts [16] and a vertical climbing technology with a large payload capacity in complex environments [4]. The adhesive property and robotic demonstrations make it straight forward for a mobile robot to use TPAs to initiate a dragline with attachment to any solid surface. Furthermore, the adhesive property and thermoplastic property of TPAs are repeatable [4], which makes them potentially recyclable. The technology presented in the paper focuses on thermoplastic dragline formation during locomotion.

2. Materials and methods

2.1. A dragline-forming mobile robot

A robot is designed and prototyped to demonstrate the feasibility of the technology (see figure 1(*b*)). The robot weighs about 185 g and has an overall dimension of $5 \times 3 \times 18$ cm^3 (width, thickness, height). The mechanical structure of the robot mainly consists of two parts i.e. a material extrusion mechanism and a coupled deformation–locomotion mechanism as briefly introduced in section 1.

The material extrusion mechanism contains solid TPA (GG02, Dremel, USA) in a cylindrical shape (ø = 7 mm). The mechanism is minimalistic and designed to be easily integrated as a part of a robotic system at the centimetre scale like the one presented in [16], but uses linear actuation and fits smaller TPA sticks. As shown in figure 1(*b*), the solid TPA stick is linearly delivered through a heating cavity and pushed out of a nozzle. Linear delivery is converted from a dc gear motor's rotation through a ball screw fixed with a TPA stick clutch. The clutch is constrained in linear motion by a linear track, the end of which is rigidly connected with the dc gear motor (motor 1, 250:1 gear ratio, Pololu, USA) and the heating cavity. The heating cavity lies in a cylindrical aluminium block and has an opening of 7 mm in diameter at one end and a nozzle with an inner diameter of 4 mm and an outer diameter of 6 mm at the other end. The cavity is heated by six 10-Ω power resistors connected in parallel and inserted in the block around the cavity. The TPA stick is held by the clutch at one end and inserted into the aluminium cavity at the other end through a silicone tube for leakage prevention. The maximal travel along the linear track is 10 cm.

The deformation–locomotion mechanism consists of two geometrically identical cylindrical wheels with a diameter of 12 mm, which are contained in a box. As illustrated in figure 2, one of the wheels is fixed on the output shaft of a second dc gear motor (motor 2, 1000:1 gear ratio, Pololu, USA), and the shaft is fixed on two opposite walls of the containing box. The second wheel is attached around a second shaft which can move linearly on a track with a fixed length on the two walls. The end points of the latter wheel's shaft are attached to the box with springs, which pull the wheel towards the centre of the mechanism. The track constraints this wheel to move along a linear route while springs allow it to passively adjust to the variable diameter of the formed dragline. The spring force is in a linear relation with the distance between the two wheels, or in other words with the diameter of the formed dragline. The force gives the normal force which generates the friction between the formed dragline and the wheels (denoted as f in a free body diagram in figure 3), enabling the robot to hold onto the formed dragline when being static (static friction), or move without free fall in the case of descending (kinetic friction). During movement, the mechanism enables the robot to elongate extruded material at the same time as moving along a formed dragline. Elongation of the material is enabled by tensile stress from adhesion forces to the nozzle at one end and to the formed segment of the dragline at the other end. The reaction force of adhesion on the robot is denoted as F in figure 3.

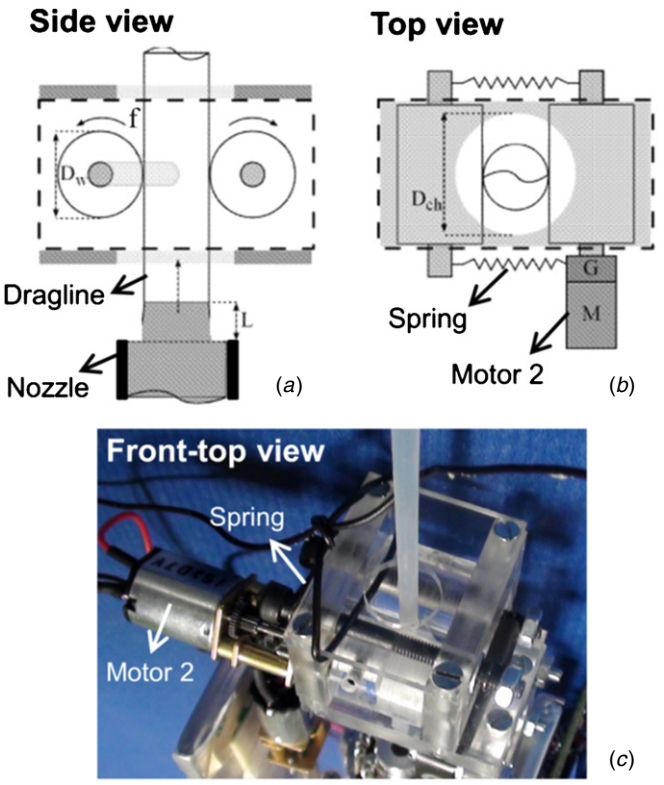

Figure 2. A coupled locomotion–deformation mechanism based on two wheels. (*a*) A schematic showing the side view. *Dw* is the cross-sectional diameter of the wheels, f is revolutions per unit time for motor 2. (*b*) A schematic showing the top view. (*c*) A view from the front-top of the mobile robot during dragline formation.

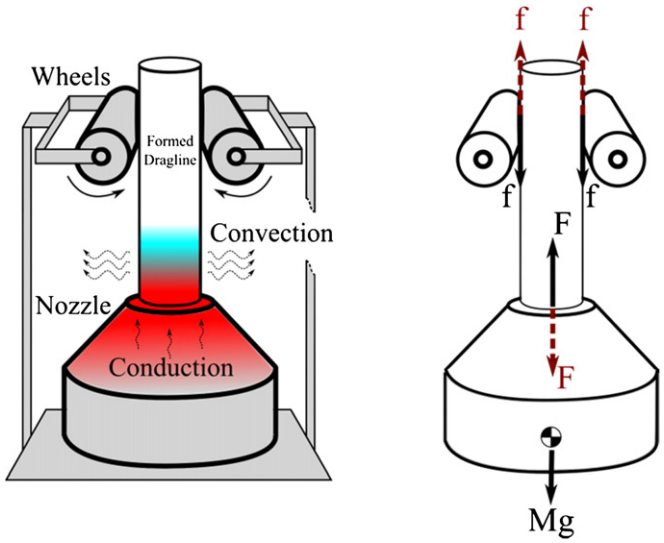

Figure 3. A schematic diagram showing the forces acting on the robot and on the dragline, as well as the two mechanisms of heat exchange. (Left) Dashed straight arrows indicate conduction and solid curved arrows indicate convection. (Right) Frictional force between the two wheels of the robot and the dragline is denoted as f, and the adhesion force between the nozzle of the robot and the dragline is denoted as F. Black solid arrows indicate forces on the robot, while red dashed arrows indicate forces on the dragline.

The two parts are arranged in such a way that the deformation–locomotion mechanism is on the upper body

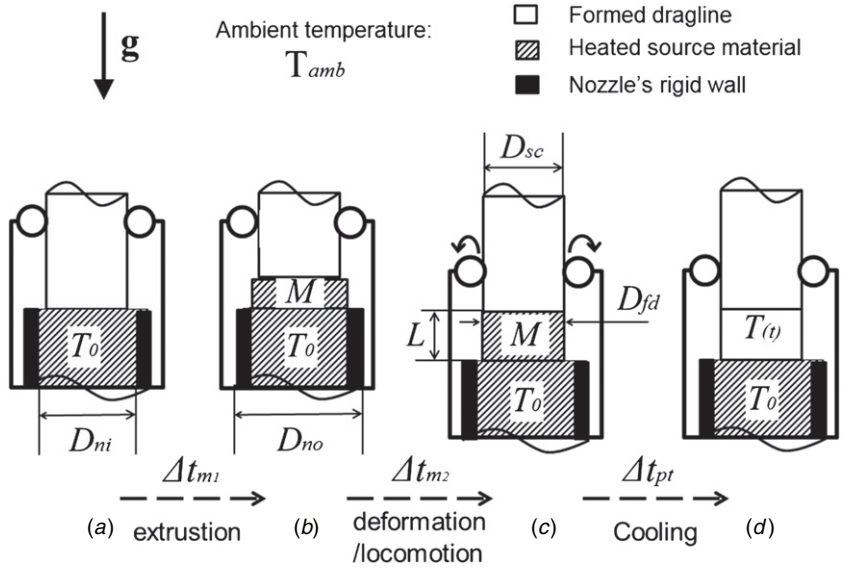

Figure 4. A control diagram of descending locomotion with dragline formation based on thermoplastic spinning. The controller consists of repetitions of a sequence of discrete events including extrusion of source material (*a*) and (*b*), deformation of extruded material into a certain cross section which may be coupled with locomotion (*b*) and (*c*), and phase transition through cooling (*c*) and (*d*). More specifically, a certain mass of source material M is extruded and deformed at an initial temperature T_0 into a dragline segment with a cross-sectional diameter of D_{fd} and a length of L. The dragline segment is then cooled with thermodynamics $T(t)$. Each event lasts a duration of Δt_{m1}, Δt_{m2} and Δtpt.

Table 1. Specification of the mobile robot.

Mass (g)	185
Dimension (width, thick, height) (cm^3)	5 × 3 × 18
Degrees of freedom	2
Extrusion temperature (°C)	65–75
Power consumption (W)	4.8
Battery life with the above power (min)	45
Average descending speed with dragline formation ($cm\ min^{-1}$)	5.13
Longest dragline (m)	0.82
Range of diameter of dragline (mm)	1.17–5.27

of the robot, and the material extrusion mechanism is on the lower body. They are connected by a rigid piece so that the exit of the extrusion nozzle is placed at a distance of 3 cm under the bottom of the deformation–locomotion mechanism. The distance determines the maximal length of the dragline before it gets held by the two wheels, which could be seen as comparable to the distance from the further end of the duct in a spider to its fourth pair of legs. A fan is attached to the connecting piece so that forced convection for cooling is possible when needed. An electronics unit including two Lithium-Polymer batteries (ICP543759PMT, Renata, Switzerland), two motor drivers (Dual MC33926, Pololu, USA), and a microcontroller board (Arduino Pro Mini, Italy) is placed on the two sides of the extrusion mechanism to ensure the lateral balance of the robot. A summary of the robot is detailed in table 1.

2.2. Thermoplastic spinning of a dragline

Thermoplastic spinning of draglines can be mathematically represented by three models, i.e. an extrusion model, a deformation model, and a thermodynamics model. The extrusion model explains the dependence of material mass flow rate on control parameters such as the shear stress exerted by an actuator e.g. motor 1, and design parameters such as the diameter of the nozzle, etc. This dependence has been previously proposed based on Newtonian fluid (further detail may be found in [16]). Once a constant mass flow rate k is determined, the mass M within a duration of extrusion Δt_{m1} can be obtained:

$$M = k\Delta t_{m1}. \tag{1}$$

The deformation model describes the dependence of dragline thickness on parameters such as material mass flow, and the speed and duration exerted by an actuator e.g. motor 2, etc. Deformation here means elongation of the extruded material along the axis of movement, so that a certain diameter of a dragline may be reached. Elongation of newly extruded material is caused by the tensile stress when the two wheels pull the structure they hold, e.g. the already formed part of dragline, away from the nozzle. In other words, the tensile stress results adhesion force on the cross-section of the structure and the cross-section of the exit of the nozzle (the reaction force of which on the nozzle/robot is shown in figure 3 and denoted as F). In the model, it is assumed that the tensile stress is always sufficient, thus no plastic solid model such as a Bingham model is considered.

Assuming elongation of a given mass of the extruded material M is isochoric and dragline has a round cross section, as illustrated in figure 4 the geometrical relationship between the length of the material L after deformation and the diameter of the cross section D_{fd} is:

$$D_{fd} = 2\sqrt{\frac{M}{\pi \rho L}} \tag{2}$$

where ρ is a constant representing the density of the material. Note that D_{fd} is upper bounded by the outer diameter of the

nozzle (D_{no} in figure 4) and the diameter of the structure that the two wheels hold on to (D_{sc} in figure 4), because the two cross-sections carry the stress that is needed for elongation. Since the deformation and locomotion is coupled (section 2.1), the length of the material L after deformation equals the rotational distance of the two wheels when slip is negligible. Thus

$$L = \pi D_w f \Delta t_{m2} \tag{3}$$

where Dw is the cross-sectional diameter of the wheels, f is revolutions per unit time for motor 2, and Δt_{m2} is the duration of the movement of motor 2, as illustrated in figure 2(a). From equations (1)–(3), the dependence of the diameter of the cross section on duration of extrusion and duration of deformation is clarified.

The thermodynamics model explains the temperature-dependent phase-transition process in an elongated dragline segment, which corresponding to the subprocess of (c) and (d) in figure 4. Phase transition of the source material from plastic to solid is realized by cooling. Its thermodynamics may be modelled with Newton's cooling law for convection and Fourier's law for conduction (the two mechanisms of heat exchange is indicated in figure 3). When temperature gradient is negligible within the material after being elongated, temperature $T(t)$ of the middle point of the material may be approximated as:

$$cM\frac{\mathrm{d}T(t)}{\mathrm{d}t} = -hA_{\mathrm{conv}}(T(t) - T_{\mathrm{amb}}) + \frac{2KA_{\mathrm{cond}}}{L}(T_0 - T(t)) \tag{4}$$

where c is a constant representing the specific heat capacity of the material, h is a constant representing the convective heat transfer coefficient, K is a constant representing the thermal conductivity of the material, T_{amb} and T_0 are constants representing the temperature of the ambient environment and the nozzle for extrusion, and A_{conv} is surface area of heat being convected and A_{cond} is surface area of heat being conducted. In the case of a cylindric thread, A_{conv} corresponds to the outer surface of the cylinder while A_{cond} corresponds to the cross section:

$$A_{\mathrm{conv}} = \pi D_{fd} L$$

$$A_{\mathrm{cond}} = \frac{\pi {D_{fd}}^2}{4}.$$

Assuming deformation occurs immediately after extrusion, the initial temperature of the material $T(t = 0)$ can be considered the same as T_0, and the equation can be solved:

$$T(t) = C_0 - C_1 \mathrm{e}^{-C_2 t} \tag{5}$$

where

$$C_0 = \frac{KT_0 D_{fd} + 2L^2 T_{amb} h}{2hL^2 + KD_{fd}}$$

$$C_1 = \frac{2L^2 h(T_{amb} - T_0)}{2hL^2 + KD_{fd}}$$

$$C_2 = \frac{2(2hL^2 + KD_{fd})}{L^2 cD_{fd}\rho}.$$

2.3. Robotic locomotion with dragline formation

Descending from a solid hanging structure is taken as a case study to show the feasibility of the robot locomotion with dragline formation, which mimics spiders falling with a dragline in a controlled way (figure 1(a)). To initiate descending, the robot first holds onto an existing structure that could be grabbed by the two wheels, e.g. a cable or a pole hanging over a free-space. The tip of the structure shall be in contact with the exit of the nozzle in the robot, so that extruded TPA at the initial stage could adhere to the structure. Locomotion is then controlled in an open-looped manner with a sequence of discrete events including extrusion, deformation/movement and phase transition. As illustrated in figure 4, in the event of extrusion and deformation/movement, motor 1 and motor 2 are turned on for duration of Δt_{m1} and Δt_{m2} respectively. Extrusion generates material which slightly pushes the formed dragline between the wheels and nozzle, but since motor 2 does not move the wheels during extrusion, the dragline in between bends a little bit rather than pushes the robot downwards. The bending is insignificant and can be quickly straightened during deformation where motor 2 is turn on to move the wheels. In the event of phase transition which lasts Δtpt, both motors are turned off and elongated material cools to a certain lower temperature in the open air and form a solid dragline. The open-loop controller is preprogrammed into the microcontroller board.

To assess the performance of the mobile technology, experiments have been conducted to measure the phase transition time as well as variability and repeatability of dragline diameter. In all experiments, the ambient temperature was room temperature, and the extrusion temperature of the TPA was set at 65–75 °C because within the range the material is sufficiently adhesive/cohesive and plastic. The robot started by holding onto a hanging thread of TPA as the solid structure in the environment.

For phase transition, the dependence of cooling time on the mass of extruded material is studied. Three values of mass were extruded and immediately deformed into a given diameter of 4 mm. The temperature change of the formed dragline segment was measured by an external thermal imager (TIM 160, Micro-Epsilon, Germany) with a sampling rate of 120 Hz. The measuring point was set at the middle point of the dragline section, which corresponds to 1.5, 2.5, and 3.5 mm above the nozzle exit for the three cases.

Regarding variability of the dragline diameter, two sets of experiments were carried out where the mass of extruded material and the final length of elongation are varied respectively. In the first set of experiment the mass of extruded TPA was varied by turning on motor 1 for a 100% duty cycle for duration Δt_{m1} between 0.3 and 2.7 s. Elongation was kept the same by turning on motor 2 for a 100% duty cycle for $\Delta t_{m2} = 0.15$ s. In the second set of experiment, Δt_{m1} was kept with a 100% duty cycles for 1.5 s, while final length of elongation was varied by setting Δt_{m2} with a 100% duty cycle between 0.05 and 0.25 s. Five trials were made for each Δt_{m1} in the first set of experiment or Δt_{m2} in the second set. One minute after each trial ($\Delta tpt =$ 60 s) the formed dragline segment was removed from the

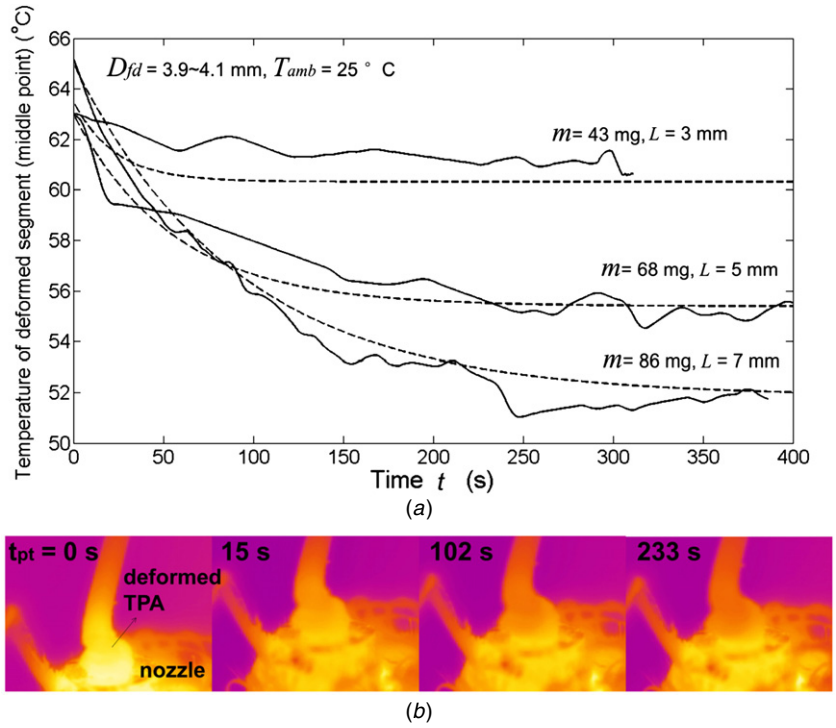

Figure 5. Thermodynamics in thermoplastic spinning of dragline segments. (*a*) A thermodynamics model showing the dependence of cooling phase transition time of a segment on the mass of extruded material in that segment. The model has been experimentally validated with TPA segments with the same cross sectional area of 4 mm. (*b*) Snapshots from the thermal imager showing the nozzle and the segment just above the exit of the nozzle in one of the trials in the experiment (the lowest curve in (*a*)).

Table 2. Constants for models.

Density ρ of the TPA (kg m^{-3})	0.98×10^3
Specific heat capacity c of the TPA (J (kg °C)$^{-1}$)	2500
Thermal conductivity K of the TPA (W (m °C)$^{-1}$)	0.45
Heat transfer coefficient h of open air (W (m^2 °C)$^{-1}$)	9

robot and the mass and diameter were measured with a high-precision scale (Voltcraft PS-20) and a digital Vernier scale.

In terms of repeatability, 15 trials containing a number of repetitions of the complete event sequence were carried out. Δt_{m1} was varied between 0.2 and 2.0 s and Δt_{m2} was varied between 0.05 and 0.15 s. Repeatability was quantified by relative deviation in cross-sectional diameters of segments along single draglines formed within each repetition. Therefore after each trial, diameters for each segment along the formed dragline were measured with a digital Vernier scale and compared to the theoretical value.

3. Results

Figure 5(*a*) shows the experimental result of the dependence of cooling time on the mass of extruded material. A TPA mass of 43, 68, and 86 mg was extruded and deformed into a diameter of 3.9–4.1 mm. The dashed lines show theoretical approximation based on the thermodynamics model, and the parameters used for the model are indicated in table 2 which are within the realistic range obtained from product datasheet and literature [18]. It took approximately 180 s for the temperature of the dragline segments to reach a steady state. The steady state was not room temperature because of continuous energy input from the nozzle. This is further visualized by snapshots from the thermo imager in figure 5(*b*) where the colour of deformed TPA gradually changes to darker. Given the same diameter, the temperature in the steady state is lower for larger amount of TPA due to the resulting larger surface area of thermal convection. This result indicates that as long as the diameter of the dragline is the same, the more TPA extruded and deformed at a given temperature, the faster it cools. This observation may be explained by the fact that the more TPA extruded, the more distant the central point of the elongated dragline segment is from the nozzle given the same diameter. The result also helps setting phase transition duration Δtpt in the experiment of diameter variability, in which case the cooling time was set to minute scale. When several repetitions of the process present, Δtpt could be set to a much smaller value, since further cooling of a formed dragline segment occurs when it is being moved away from the nozzle towards the wheels. For example, in the experiment of diameter repeatability, it was possible to set Δtpt to only 3 s.

Figure 6 shows the results from the two sets of experiment for diameter variability. The experiment conditions and results are also summarized in table 3. For the first set of experiment as in figure 6(*a*), theoretical estimation from the deformation model is also plotted with M estimated from $k\ \Delta t_{m1}$ with an empirical mass flow rate $k = 6.75$ mg s^{-1}, and L calculated from (2) with $f = 14$ rpm (100% duty cycle for motor 2). It can be seen that the model fits experimental data very well. Figure 6(*b*) shows the diameter variation from the second set of

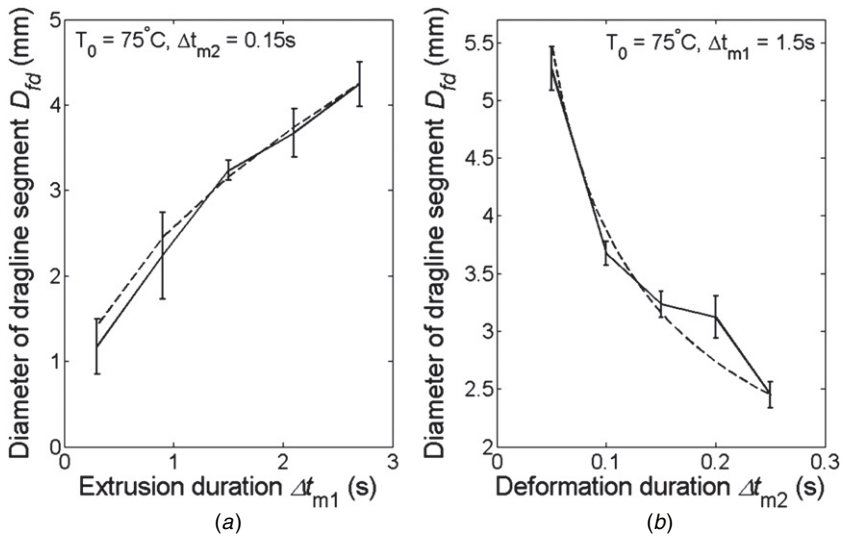

Figure 6. Variability in diameter of formed draglines. (*a*) Results from varying the extrusion duration. (*b*) Results from varying the deformation duration. Theoretical values from (1) are on the dashed lines.

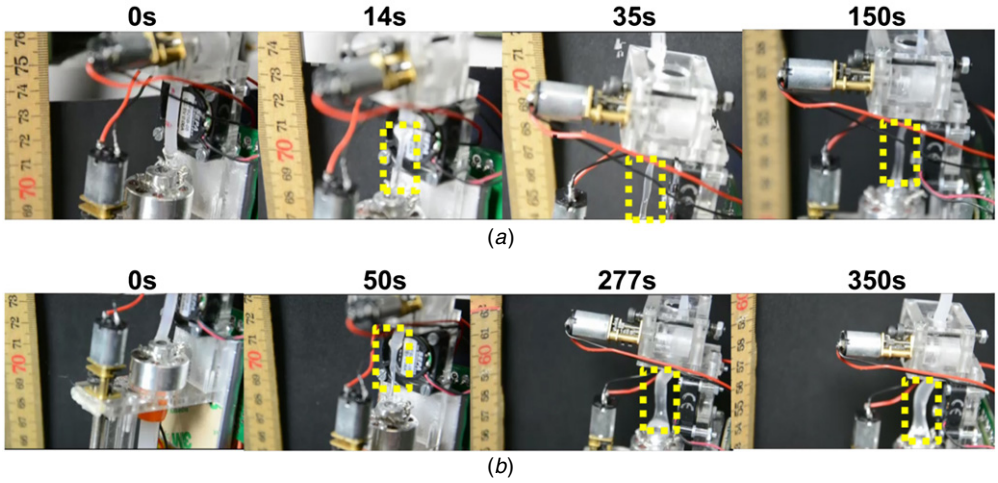

Figure 7. Snapshots of thermoplastic dragline formation during descending locomotion under different control parameters. (*a*) $\Delta t_{m1} = 0.2$ s and $\Delta t_{m2} = 0.05$ s. (*b*) $\Delta t_{m1} = 1.5$ s and $\Delta t_{m2} = 0.1$ s. The process was initiated at time 0 s with the two wheels grabbing a solid structure of a hanging TPA thread. Under the condition in (*a*) a thinner thread with a mean cross-sectional diameter of around 2 cm was formed, and under the condition in (*b*) a thicker thread with a mean cross-sectional diameter of around 4 cm was formed. The forming dragline segments are indicated within dashed yellow rectangular regions. The background ruler was fixed vertically in the environment and the change in reading indicates movement of the robot along the formed dragline (for example, the reading of 70 or 60 moved upwards, indicating the robot was descending).

Table 3. Experiment results for diameter variability.

	Δt_{m1} (s)	Δt_{m2} (s)	Diameter (mm)
First set of experiment	0.3	0.15	1.17 ± 0.32
	0.9		2.24 ± 0.51
	1.5		3.23 ± 0.11
	2.1		3.67 ± 0.28
	2.7		4.24 ± 0.26
Second set of experiment	1.5	0.05	5.27 ± 0.19
		0.10	3.67 ± 0.10
		0.15	3.23 ± 0.11
		0.20	3.12 ± 0.18
		0.25	2.45 ± 0.11

experiment. In the figure, theoretical estimation is also plotted with a mass of 10 mg (experimental data 10.15 ± 0.65 mg) and L calculated from (2) with $f = 14$ rpm. It can be seen that the model also follows experimental data. Overall, a diameter range of 1.17–5.27 mm has been achieved for formed dragline segments.

In terms of repeatability, all trials succeeded with more than ten repetitions of event sequence and the robot managed to move on formed draglines. A maximal value of average descending speed of 5.13 cm min^{-1} was achieved. While we have tested dragline-assisted locomotion as far as 82 cm, there is no limitation in travelling distance unless the source material is used up. Figure 7 shows snapshots of dragline formation process under two different control conditions. In figure 7(*a*), a trial (ID 13) with control parameters

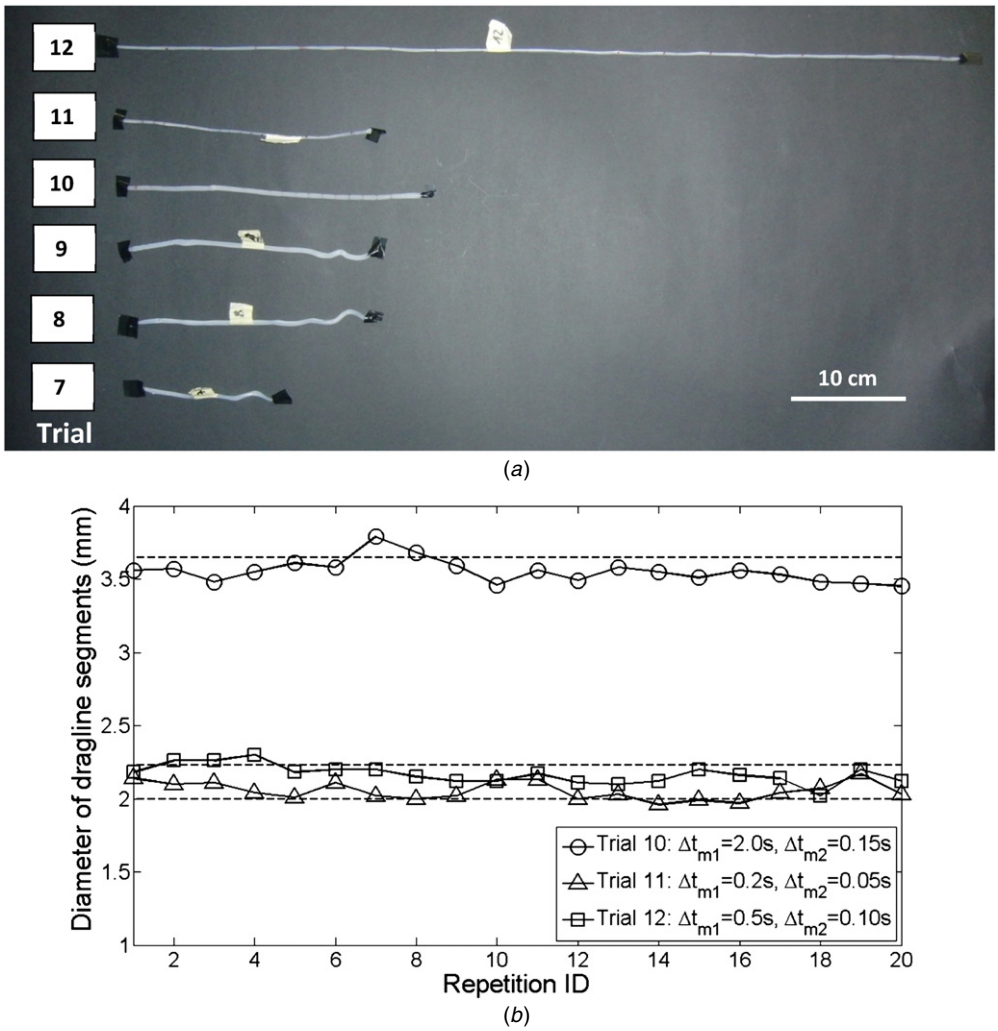

Figure 8. (*a*) Draglines formed by the robot during descending from a hanging structure. (*b*) Repeatability in diameter of formed draglines. Repeatability is quantified as the relative deviation between the diameter of dragline segments and a theoretical value. The theoretical values expected from equation (2) are plotted in dashed lines. Results suggest a relative deviation between the thinnest dragline segment and the expected diameter to be within −4%.

$\Delta t_{m1} = 0.2$ s and $\Delta t_{m2} = 0.05$ s is shown. In figure 7(*b*), a trial (ID 14) with control parameters $\Delta t_{m1} = 1.5$ s and $\Delta t_{m2} = 0.1$ s is shown. The snapshots not only show the process of thermoplastic dragline formation during descending locomotion, but also contrast the thickness of draglines under different control conditions. Figure 8(*a*) shows draglines formed by the robot while descending in six of the trials (ID $7 \sim 12$). Figure 8(*b*) shows quantitative data of repeatability from three of the trials, in which the diameters were 3.55 ± 0.08 mm, 2.17 ± 0.06 mm and 2.05 ± 0.06 mm respectively. The theoretical value expected from equation (2) for each trial is indicated by a dashed line. The result suggests a maximum of relative negative deviation of −4% between the thinnest segment and the expected value. The deviation came from TPA extrusion and deformation, and physical interactions between the formed dragline segments and the deformation–locomotion mechanism. The relative deviation shows a good repeatability of dragline formation during locomotion and it is important for setting safety margins given a target payload.

4. Discussion

The range of diameter and relative deviation for repeatability directly determine the payload capacity of the mobile technology, when it is assumed that adhesion force between the dragline and a solid surface in the environment is sufficient and the force between the holding mechanism and the dragline is always enough. For a given source material, its ultimate tensile strength at room temperature is given, then the payload capacity can be estimated. For example, the type of TPAs used in the study has ultimate tensile strength of around 5 MPa, which gives an estimation of payload potential of 0.36–10.94 kg with the achieved range of diameter. Stronger thermoplastics may be used as source material to further increase the payload range. However, the intrinsic inter-dependence between physical properties of material needs to be clarified, such as that between viscosity and strength or between softening point and strength, etc, so that control parameters could be adjusted.

Regarding self-sufficiency of the robot, it is determined by both the energy storage in the batteries and the material

storage of source TPA. The latter determining factor does not present in conventional mobile robots and worth discussing. TPA is generally reusable in terms of both thermoplasticity and adhesion [4]. However it requires additional mechanisms onboard a mobile robot to retrieve a formed dragline and reuse it as source material, which will largely increase the complexity of the system. In the current setup the maximal volume of the source TPA is determined by the maximal travel along the linear track and the diameter of the solid TPA stick, since the linear delivery for extrusion is only one-way. If an external TPA storage can be included, the self-sufficiency of the entire robotic system can be significantly improved, in which case only a reset mechanism will be needed to reset the clutch back to its origin once the maximal travel has been reached by linear delivery.

From the perspective of control engineering, the present open-looped controller based on a sequence of discrete events is unlikely to be the optimal for variability and repeatability of dragline formation, neither for the locomotion speed. For example, it is imaginable that the speed can be increased if extrusion, deformation/locomotion and cooling happen at the same time in a continuous manner. Since cooling takes more time than extrusion or deformation/locomotion, the speed may be further increased if cooling is made faster. It is also expected that continuous dragline formation and locomotion will avoid unnecessary start and stop of motors, which was the cause of relative deviation between repetitions of the event sequence. In order to achieve a controller for locomotion with continuous dragline formation, the relation between mass flows from extrusion to deformation/locomotion needs to be clarified, and its influence on the thermodynamics of different dragline segments needs to be understood. That will be the next step work for a model-based open-loop controller.

The case study of descending locomotion along a formed dragline provides evidence and quantitative analysis of the proposed approach and may be extended and applied to 3D locomotion with formation of multiple draglines and eventually grids. Legged technology is needed to replace the double-wheel mechanism for that purpose, so that the robot may move away from a single dragline to a solid surface or a second dragline. Part of the legs should enable the robot to adhere to both a dragline and a surface. A potential simple solution to this is to use gecko-inspired dry adhesives on the legs. Since the adhesive strength of such adhesives is relatively low (see a quantitative comparison in [4]), the contact area on the legs should be maximized to provide sufficient adhesion force. One of the possible ways for a robot with legs to form a grid is to start with a single vertical dragline. The robot then climbs back up the dragline and reaches the solid structure and moves on it with legs to where the second vertical dragline is targeted. When a number of vertical draglines have been made in this way, the robot may span its legs between them and form horizontal draglines with additional degrees of freedom of the nozzle to move horizontally. Thermoplastic formation of horizontal draglines has been proven feasible without supporting material [19]. When the grid is formed from multiple vertical and horizontal draglines, 3D positioning is possible and this could partially mimic the web-building behaviour of spiders.

The reported result shows a 185 g mobile robot is able to form draglines with a thickness of 1.17–5.27 mm. Compared to a spider weighing a couple of hundred milligrams and being able to produce draglines with thickness of a few micrometres [10], the robot is an up-scaled physical model of the real spider by three orders of magnitude. When the locomotion of the robot is improved both in speed and continuity such that it resembles the real spider [20, 21], the physical model may be used for studying spider behaviours associated with draglines. For example, one of the open questions is the cause and measurement of initial stress that moves the protein molecules in a nematic state from the gland into the duct. That is not trivial to find out in a living spider, and the controlled physical model may help as long as the polymeric flows in the spider and in the robot are comparable and scalable. Another interesting question is the function of the valve at the end of the duct in dynamics of spider descending and jumping. For example, it has been observed that jumping spiders have a forward pitch movement of their body towards the end of a ballistic jump [22]. That is believed to be associated with the valve acting as a brake but no quantitative modelling has been done. A modified robot with additions of a valve and a jump-launching mechanism may shed light on this.

Acknowledgments

We thank Milan Jovic for improving the design of the robot and Cinzia Peruzzi for collecting the data for validation of the thermodynamics model. The work was funded by the Swiss National Science Foundation Professorship grant no PP00P2123387/1, and the ETH Zurich Research grant no ETH-23-10-3.

References

[1] Dalvand M M and Moghadam M M 2006 Stair climber smart mobile robot (MSRox) *Auton. Robot.* **20** 3–14

[2] Haynes C G, Khripin A, Lynch G, Amory J, Saunders A, Rizzi A A and Koditschek D E 2009 Rapid pole climbing with a quadrupedal robot *ICRA'09: Proc. 2009 IEEE Int. Conf. on Robotics and Automation, (Kobe, Japan)* pp 2767–72

[3] Hirose S, Nagakubo A and Toyama R 1991 Machine that can walk and climb on floors, walls and ceilings *Proc. 5th Int. Conf. on Advanced Robotics, (Pisa, Italy, 19–22 June)* pp 753–8

[4] Wang L, Graber L and Iida F 2013 Large-payload climbing in complex vertical environments using thermoplastic adhesive bonds *IEEE Trans. Robot.* **29** 863–74

[5] Krishna M, Bares J and Mutschler E 1997 Tethering system design for Dante II *Proc. 1997 IEEE Int. Conf. on Robotics and Automation, (Albuquerque, NM, 20–25 April)* pp 1100–5

[6] Kuntze H-B and Haffner H 1998 Experiences with the development of a robot for smart multisensoric pipe inspection *Proc. 1998 Int. Conf. on Robotics and Automation, (Leuven, Belgium)* pp 1773–8

[7] Molfino R, Armada M, Cepolina F and Zoppi M 2005 Roboclimber the 3 ton spider *Ind. Robot.* **32** 163–70

[8] Bonani M, Magnenat S, Retornaz P and Mondada F 2009 The Hand-Bot, a robot design for simultaneous climbing and manipulation *Proc. 2nd Int. Conf. on Intelligent Robotics and Applications, (Singapore)* pp 11–22

[9] Desbiens A L, Asbeck A T and Cutkosky M R 2011 Landing, perching and taking off from vertical surfaces *Int. J. Robot. Res.* **30** 355–70
[10] Vollrath F 1999 Biology of spider silk *Int. J. Biol. Macromol.* **24** 81–8
[11] Vollrath F, Madsen B and Shao Z 2001 The effect of spinning conditions on the mechanics of a spider's dragline silk *Proc. R. Soc. Lond.* B **268** 2339–46
[12] Wilson R S 1962 The control of dragline spinning in the garden spider *Q. J. Micr. Sci.* **104** 557–71
[13] Vollrath F and Knight D P 2001 Liquid crystalline spinning of spider silk *Nature* **410** 541–8
[14] Teule F, Miao Y G, Sohn B H, Kim Y S, Hull J J, Fraser M J Jr, Lewis R V and Jarvis D L 2012 Silkworms transformed with chimeric silkworm/spider silk genes spin composite silk fibers with improved mechanical properties *Proc. Natl Acad. Sci. USA* **109** 923–8
[15] Sancaktar E 2011 Classification of adhesive and sealant materials *Handbook of Adhesion Technology* ed L F M da Silva, A Oechsner and R D Adam (Heidelberg: Springer) p 12
[16] Wang L and Iida F 2012 Physical connection and disconnection control based on hot melt adhesives *IEEE-ASME Trans. Mechatronics* **18** 1397–409
[17] Emile O, Le Floch A and Vollrath F 2006 Biopolymers: shape memory in spider draglines *Nature* **440** 621
[18] Zarandi M B, Bioki H A, Mirbagheri Z, Tabbakh F and Mirjalili G 2012 Effect of crystallinity and irradiation on thermal properties and specific heat capacity of LDPE & LDPE/EVA *Appl. Radiat. Isot.* **70** 1–5
[19] Leach D, Wang L, Reusser D and Iida F 2013 *In situ* thermoplastic thread formation for robot built structures *Proc. 16th Int. Conf. on Advanced Robotics (Montevideo, Uruguay, 25–29 November 2013)* at press
[20] Ortlepp C S and Gosline J M 2004 Consequences of forced silking *Biomacromolecules* **5** 727–31
[21] Boutry C, Rezac M and Blackledge T A 2011 Plasticity in major ampullate silk production in relation to spider phylogeny and ecology *PLoS One* **6** e22467
[22] Hill D E 2006 Targeted jumps by salticid spiders (Araneae, Salticidae, Phidippus) http://peckhamia.com/epublications.html